We are IntechOpen,
the world's leading publisher of Open Access books
Built by scientists, for scientists

6,900
Open access books available

186,000
International authors and editors

200M
Downloads

154
Countries delivered to

Our authors are among the

TOP 1%
most cited scientists

12.2%
Contributors from top 500 universities

BOOK CITATION INDEX
CLARIVATE ANALYTICS
INDEXED

WEB OF SCIENCE™

Selection of our books indexed in the Book Citation Index
in Web of Science™ Core Collection (BKCI)

Interested in publishing with us?
Contact book.department@intechopen.com

Si-Based ZnO Ultraviolet Photodiodes

Lung-Chien Chen

Additional information is available at the end of the chapter

http://dx.doi.org/10.5772/48825

1. Introduction

Semiconductor-based ultraviolet (UV) photodiodes have been continuously developed that can be widely used in various commercial, civilian areas, and military applications, such as optical communications, missile launching detection, flame detection, UV radiation calibration and monitoring, chemical and biological analysis, optical communications, and astronomical studies, etc. [1-2]. All these applications require very sensitive devices with high responsivity, fast response time, and good signal-to-noise ratio is common desirable characteristics. Currently, light detection in the UV spectral range still uses Si-based optical photodiodes. Due to the Si-based photodiodes are sensitive to visible and infrared radiation, the responsivity in the UV region is still low [3-5]. To avoid these disadvantages, wide-bandgap materials (such as diamond, SiC, III-nitrides and wide-bandgap II–VI materials) are under intensive studies to improve the responsivity and stability of UV photodiodes, because of their intrinsic visible-blindness [6].

Among them, zinc oxide (ZnO) is another wide direct bandgap material due to its sensitive and UV photoresponse in the UV region [7-9]. ZnO has attracted attention as a promising material for optical devices, owing to its large direct band gap energy of 3.37 eV and a large exciton binding energy of 60 meV at room temperature compared to other II-VI semiconductors [10-12]. Therefore, ZnO is promising for use in light-emitting diodes (LEDs), laser diodes (LDs), ultraviolet (UV) detection devices [12-15]. Several deposition methods have been employed for the growth of ZnO layers, including metal-organic chemical vapor deposition (MOCVD), molecular beam epitaxy (MBE), pulsed laser deposition (PLD), sol-gel and spray pyrolysis [16-20]. The synthesis of *p*-type ZnO films with acceptable stability and reproduci-

bility by means of indium and nitrogen codoping or other group-III elements and nitrogen codoping has recently been demonstrated [21-24].

Since the quality of ZnO materials plays a key role in determining the performance of UV photodiodes. This chapter reviews the recent progress in Si-based heterostructure (UV) photodiodes, including p-ZnO/n-Si UV photodiodes, and p-ZnO/SiO$_2$ ultrathin interlayer/n-Si UV photodiodes. Furthermore, the optoelectronic and the magneto-enhanced characteristics (so called magneto-optical multiplication effects) of UV photodiode placed in a strong magnetic field were elucidated.

2. ZnO/Si UV photodiodes

Fabrication of a p-ZnO/n-Si heterojunction photodiode was reported [25]. An N-In codoped p-type was deposited on a (111)-oriented silicon substrate by ultrasonic spraying pyrolysis method. Three aqueous solution, $Zn(CH_3COO)_2$ $2H_2O$ (0.5 mol/l), CH_3COONH_4 (2.5 mol/l), and $In(NO_3)_3$ (0.5 mol/l), were as the source of zinc, nitrogen, and indium, respectively. The atomic ratio of Zn/N is 1:2 for N-doped film, and Zn/N/In is 1:2:0.15 for N-In codoped film [21]. The n-type Si (111) wafers were used as the substrates, which were etched with HCl for 5 min before deposition. The aerosol of precursor solution was generated by the commercial ultrasonic nebulizer. P-type N-In codoped ZnO films were obtained by heating the substrate to 650 C, and were subsequently studied by Hall measurement. The hole concentration and mobility of p-ZnO were around 1×10^{17} cm^{-3} and approximately 46 cm^2/V-s, respectively. P-ZnO/n-Si structures were then fabricated. The Ni/Au ohmic contact layer was evaporated onto the p-type ZnO film as the anode electrode, and a Ti/Pt/Au electrode was formed on the backside of the n-type Si substrate as the cathode electrode. Then, the cross section of the completed structure is shown in Figure 1. The ZnO film with thickness of about 1.3 μm was formed on silicon substrate.

Figure 2(a) shows the plots of the I-V characteristics of the photodiodes measured in the dark (dark current) and under illumination (photocurrent, λ=530 nm) at reverse biases from 0 to 1 V. As shown in Fig. 2(a), it was found the photocurrent approximately 3.9×10^{-7} A and the dark current was approximately 8.87×10^{-9} A at a bias of 1 V. Therefore, it was found that a photocurrent to dark current contrast ratio is around two orders of magnitude. Figure 2(b) shows the plot of responsivity as a function of the wavelength for a p-ZnO/n-Si heterostructure photodiode at a bias of 1 V. The photodiodes exhibited two higher responsive regions denoted as A and B, respectively. Region A at wavelength approximately from 400 nm to 700 nm was owing to ZnO film absorption occurring through the band-to deep level [26], and region B at wavelength approximately from 700 nm to 1000 nm was owing to Si substrate absorption occurring through the band edge.
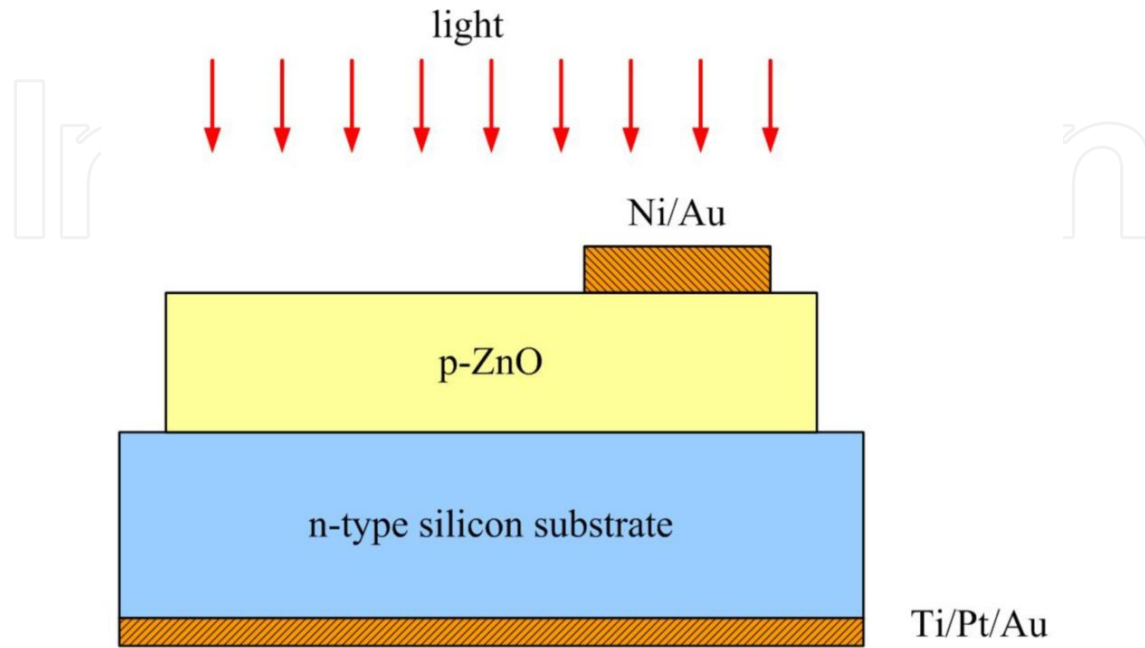
Figure 1. Schematic cross section of the completed structure. [25].

Responsivity *R* is given by [27]

$$R = I_{ph} / P_{inc} = \eta \frac{q}{h\nu} (A/W) \tag{1}$$

where I_{ph} is the photocurrent, P_{inc} is the incident power, and η, q, ν and h are the *QE*, the elec-
tron charge, the frequency of incident light, and Planck's constant, respectively. Using Eq. (1),
the values of responsivity and QE at 530 nm at biases of 1 V were 0.204 A/W and 47.73%, re-
spectively. The values of responsivity and QE at 850 nm at biases of 1 V were 0.209 A/W and
30.49%, respectively. In contrast to conventional Si-based photodetectors, the ZnO film has
been improved the responsivity in UV/blue region. However, the responsivity was degrad-
ed in near infrared region (700-1100 nm). This result means that the portion of light with high-
er energy, such as 400–500 nm, was absorbed by ZnO film and the portion of light with lower
energy, such as 800-1000 nm, can completely incident into Si substrate and was absorbed.
However, the responsivity owing to the ZnO film absorption occurring through the band-to-
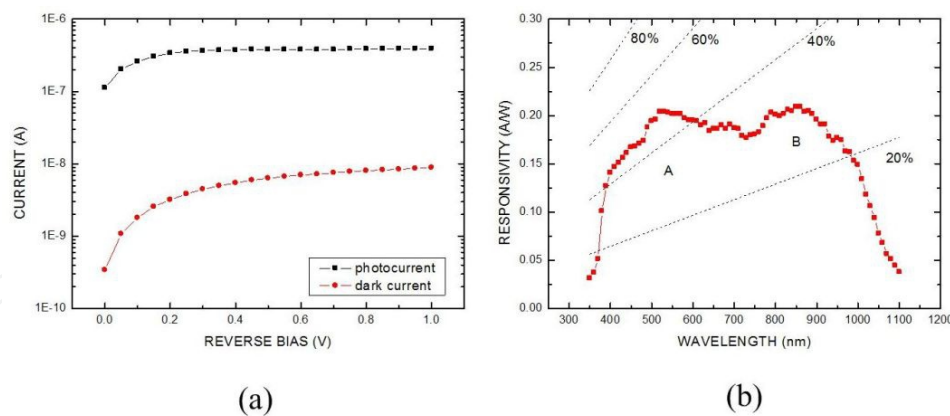band did not observe in this work.

Figure 2. a) The dark and illuminated (λ=530 nm) I-V characteristics of the *p*-ZnO/*n*-Si heterostructure photodiode. (b) The responsivity as a function of the wavelength for a *p*-ZnO/*n*-Si heterostructure photodiode at a bias of 1 V [25].
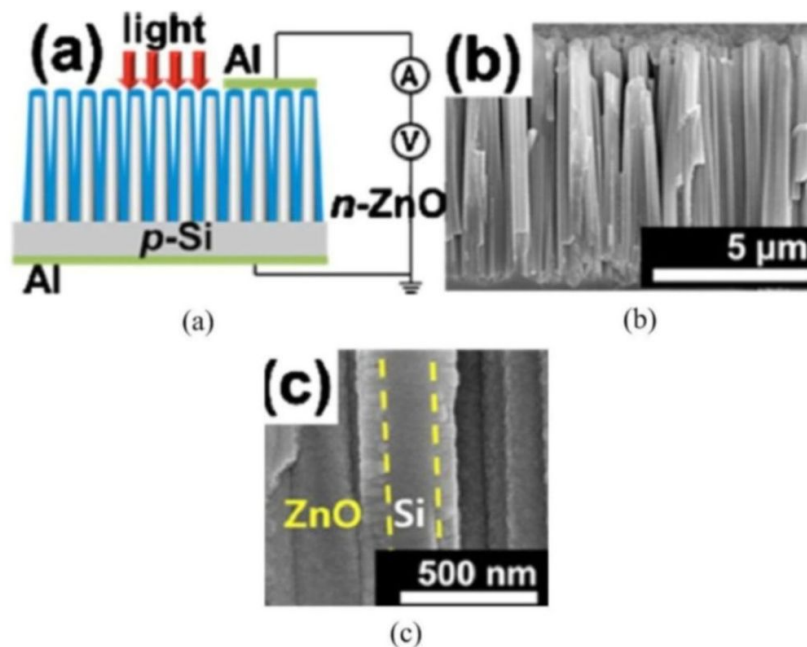

Figure 3. a) Schematic showing the configuration of the photoresponse measurement system used for the *n*-ZnO (shell)/*p*-Si (core) radial nanowire photodiodes. (b) A typical cross-sectional SEM image of the *n*-ZnO/*p*-Si NW arrays. (c) A magnified image showing the bottom region of a ZnO/Si NW [28].

Kim et al. [28] were demonstrated utilizing radial heterojunction nanowire diodes (RNDs) array consisting of *p*-Si/*n*-ZnO NW core/shell structures which were fabricated using conformal coating by atomic layer deposition (ALD). Vertically dense Si NW arrays were prepared by Ag-induced electroless etching of *p*-type Si wafers. After formation of the Si NW arrays, the ALD technique was used to conformably coat a *n*-type ZnO thin film on the high aspect ratio Si NWs, as shown in figure 3(a). The properties of long (6 μm) and short (2 μm) nanowire photodiodes, denoted as RND2 and RND6, respectively. The typical diameter of the *n*-ZnO/*p*-Si NW arrays was 350-400 nm, which consisted of a 100 nm thick shell and a 150-200

nm thick NW core. The aspect ratios of the RNDs, which were calculated using the averaged values of the lengths and diameters, were ~10 and 30 for RND2 and RND6, respectively. A magnified image showing a ZnO/Si NW, in which the ZnO shells were partly peeled off during the sample preparation. A uniform thickness of ZnO over the Si core is observed. The yellow dashed lines indicate the position of the interface between ZnO and Si, as shown in Figs. 3(b) and 3(c).

Figure 4(a) shows the photoresponsivity spectra under a forward bias of 0.5 V. It is clear the UV responsivities of RND2 and RND6 are higher than that of the planar thin film diode (PD) under a forward bias. Such as compared to a PD, a RND2 (6 µm) resulted in a ~2.7 times enhancement of the UV responsivity at λ=365 nm in the forward bias. In addition, the enhanced UV photoconductive response in ZnO NWs may be attributed to the presence of oxygenrelated hole-trap states at the NW surface [29]. As a result, RNDs can improve the UV photodetection sensitivity due to the high surface area to volume ratio. In this case, the UV responsivities at λ=365 nm were detected to be 0.23, 0.42, and 0.63 A/W for PD, RND2, and RND6, respectively. Owing to the short penetration depth, the carrier generation normally occurs near the surface. It indicates surface scattering and recombination decrease the carrier lifetime. Figure 4(b) shows the photoresponsivity spectra of RNDs compared to the PD under a reverse bias. The values of the visible/UV responsivity at λ=700 nm and 365 nm were 17.2 A/W for RND6 and 0.86 A/W for PD. It appears that the ZnO surface can be depleted by the surface oxygen absorption according to the hole-trapping mechanism [29]. Therefore, both the UV and visible photoresponsivities of the RNDs were better than that of a planar PD, owing to the enlarged surface area to volume ratio, efficient carrier collection, and improved light absorption.
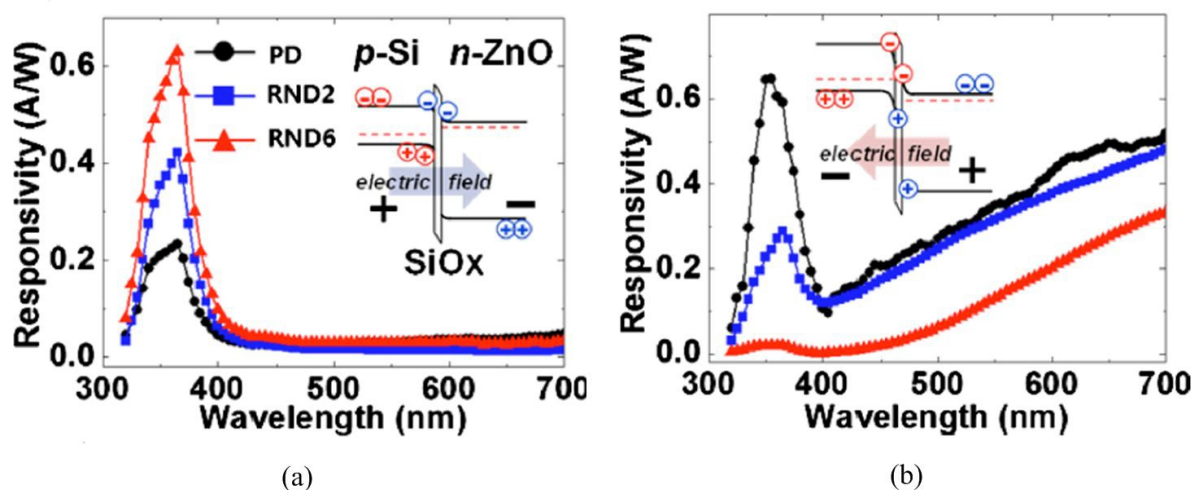

Figure 4. Photoresponsivity spectra of the RNDs and PD measured under (a) forward and (b) reverse biases. Their energy band diagrams and charge transport mechanisms are also depicted in the insets [28].

3. ZnO/SiO$_2$/Si UV photodiodes

3.1. Ultrathin SiO$_2$ films

Many the various types of photodiodes which include homojunction, heterojunction and metal-semiconductor-metal (MSM) photodiodes much attention has been paid in recent years to metal-oxide-semiconductor (MOS) structures [30-33]. An ultrathin silicon dioxide (SiO$_2$) films has been the most commonly used material for diffusion barriers and insulating layers for various applications in MOS devices due to its properties such as low defect density, high thermal stability, high resistivity, high electric insulating performance, high reliability, and reasonable dielectric constant [34,35]. In general, an ultrathin SiO$_2$ films ($\leq$ 1 nm) was formed on the silicon substrate that the silicon/SiO$_2$ interface becomes crucial for good transistor behavior. Several fabrication methods have been employed for the formed of ultrathin SiO$_2$ films, such as rapid thermal oxidation (RTO) [36], oxidation with excited molecules and ions [37,38], plasma oxidation [39,40], photo-oxidation [34,41], ozone oxidation [43], metal-promoted oxidation [44], anodic oxidation [45,46] and nitric acid (HNO$_3$) vapor oxidation [47,48] etc. When a reverse bias is applied to a MOS photodiode, the energy bands in the semiconductor bend and a potential well is formed between the oxide and the semiconductor. Electron-hole pairs generated near the junction by incident light will be stored in the potential well, and current transport occurs through the oxide layer via tunneling.

Recently, Chen et al. [49-51] reported the *p*-ZnO/SiO$_2$ ultrathin interlayer/*n*-Si substrate structure photodiodes. An ultrathin SiO$_2$ film as interlayer was formed on a (111)-oriented silicon substrate by heating the substrate in wet oxygen ambient at 650 C for 10 min to improve the performance of ZnO/Si photodiodes by inserting a SiO$_2$ ultrathin interlayer.

3.2. ZnO/SiO$_2$/Si UV photodiodes

In 2003, Jeong et al. [52] presents *n*-ZnO/*p*-Si photodiodes through use of a SiO$_2$ ultrathin oxide interlayer that unintentionally doped n-ZnO thin films were deposited on p-type Si substrates by RF magnetron sputtering. A schematic cross-section of the complete structure is shown in Figure 5 (a). The *n*/*p* heterojunction has a thin SiO$_2$ layer about 3 nm at the *n*-ZnO/*p*-Si interface and hence the photoelectrons may face a transport barrier. The result indicates that *n*-ZnO/*p*-Si photodiodes could detect UV photons in the depleted *n*-ZnO and simultaneously detect visible photons in the depleted *p*-Si. Figure 5 (b) presents the spectral responsivity curves obtained from the *n*-ZnO/*p*-Si photodiode. The responsivity of a photodiode for visible light was as high as ~0.26 A/W at 5 V and 0.4 A/W at 30 V. The UV-driven responsivity spectra are quite different, showing a noticeable increase with voltage. Higher responsivity is found for more energetic UV photons from the photodiode. For the 310 nm UV photons, the *n*-ZnO/*p*-Si photodiode shows responsivity of 0.09 A/W at 5 V and 0.5 A/W at 30 V. However, they show relatively weak response near 380 nm, which is the band gap of ZnO.
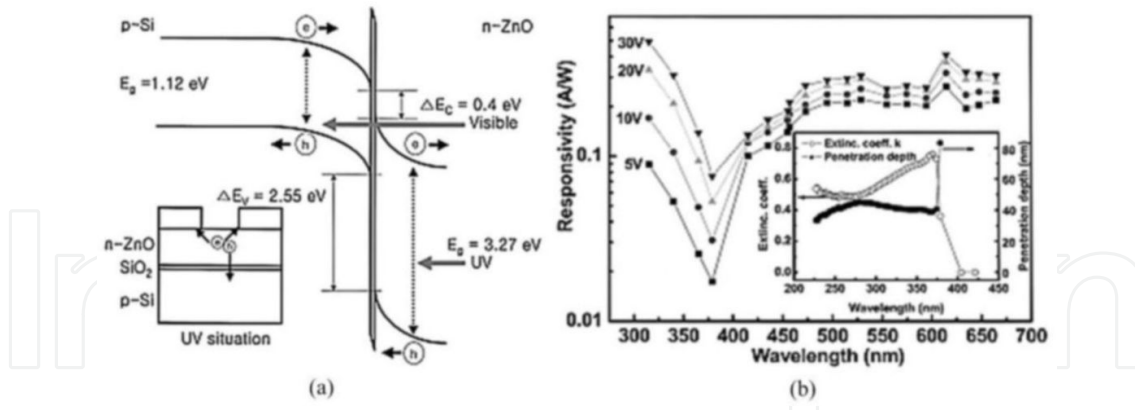
Figure 5. a) Energy-band diagram of a reverse-biased n-ZnO/p-Si structure. (b) Spectral responsivity curves obtained under the reverse biases [52].

Additionally, we found that an intermediate SiO_2 ultrathin film can improve the quantum efficiency and the responsivity by decreasing the surface state density and increase the tunneling photocurrent [49-51]. Figure 6 (a) shows a schematic cross-section of the complete structure. The inset in this figure shows a schematic cross-sectional TEM image of nanostructure p-ZnO/SiO_2 ultrathin interlayer/n-Si substrate. The ZnO film had an anomalous nano-scale columnar structure with a diameter of 50-80 nm. The ultrathin oxide layer between the ZnO film and the Si substrate had a thickness of approximately 26 Å, as estimated from the TEM image in Fig. 6(b) taking the area A in Fig. 6(a).
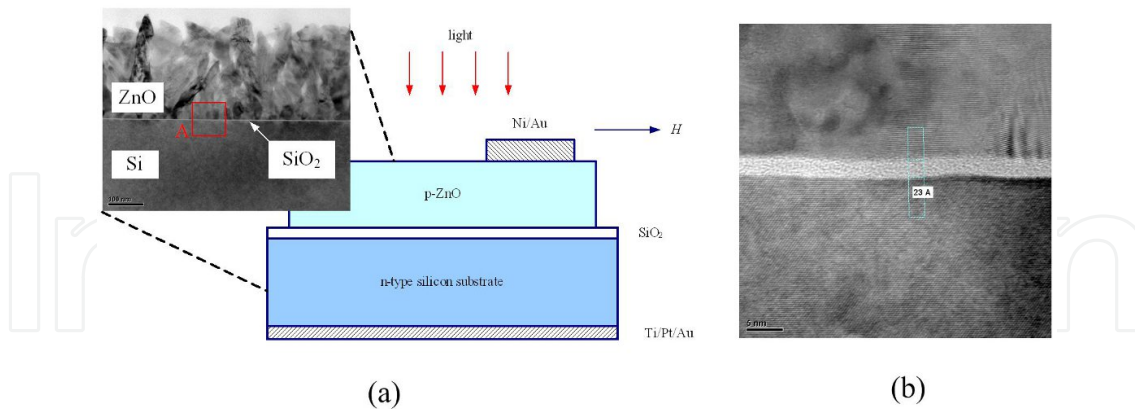

Figure 6. a) Schematic cross-section of the complete structure. (b) Cross sectional TEM image of p-ZnO/SiO_2 ultrathin interlayer/n-Si structure [49,51].

Figures 7(a) and 7(b) present a schematic band diagram to elucidate the current components. Based on Figure 7(a), the dark current can be described as [30,53]

$$J_{dark} = J_{Sp} + J_{Tp} + J_{Sn} + J_{Tn} \tag{2}$$

where J_{Sp} is the hole current through surface states, J_{Tp} is the hole tunneling current, J_{Sn} is the electron current tunneled through surface states, and J_{Tn} is the electron current through surface states. As shown in Figure 7(b), the photocurrent mechanisms can be written as

$$J_{light} = J_{Tn} + J_{Dn} + J_{Ln} + J_{Tp} + J_{Dp} + J_{Lp}$$ (3)

where J_T is the tunneling current, J_D is the current in the depletion region, and J_L is the photo-generated current. The subscripts n and p indicate electron and hole, respectively.
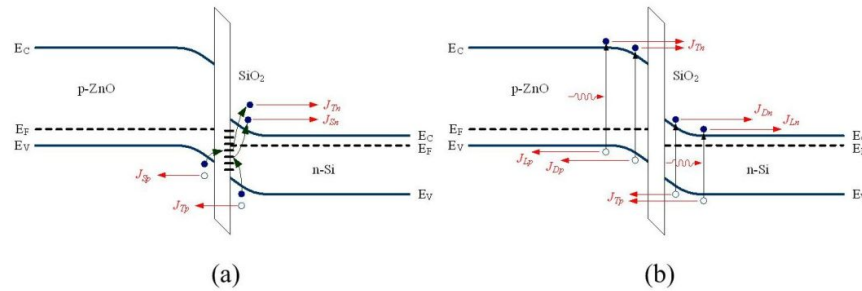

Figure 7. Schematic energy-band diagram of the p-oxide-n tunnel diode system under (a) dark and (b) illuminated conditions [49].

Figure 8(a) plots the responsivity as a function of (*I-V*) characteristics of photodiodes that were measured in the dark and under illumination (λ = 530 nm) with a 250 W xenon arc lamp at reverse biases from 0 to 1 V. At a reverse bias of 1 V, for the *p*-ZnO/*n*-Si structure, the photocurrent was ~3.9×10^{-7} A and the dark current was ~8.87×10^{-9} A. For the *p*-ZnO/SiO$_2$ ultrathin interlayer/*n*-Si structure, the photocurrent and the dark current were ~4.99×10^{-5} A and ~4.98×10^{-10} A, respectively. It can be noted that the photocurrent-to-dark-current contrast ratios improved from two orders of magnitude to five orders of magnitude. Evidently, the *p*-ZnO/SiO$_2$ ultrathin interlayer/*n*-Si structure improves the photocurrent-to-dark-current contrast ratio by passivating the surface states and enhancing the tunneling current, as shown in Figures 8(a) and 8(b).

Figure 8(b) plots the as a function of wavelength for both a *p*-ZnO/*n*-Si and a *p*-ZnO/SiO$_2$ ultrathin interlayer/*n*-Si photodiode, measured throughout this work at a reverse bias of 1 V. The photodiode responsivities can be divided into three regions of around wavelengths of 400 nm, 530 nm, and 850 nm, denoted A, B, and C. Region A, at a wavelength of around 400 nm, corresponds to excitonic absorption in the ZnO film [54,55]. Region B, which is defined as the wavelength range from about 400 nm to 700 nm, corresponds to band-to-deep level absorption in the ZnO film [26]. Region C (wavelengths between 700 nm to 1000 nm) corresponds to band edge absorption in the Si substrate. According equation (1), for the *p*-ZnO/*n*-Si structure, in region A, B, and C, the responsivity (*R*) and quantum efficiency (*QE*) were 0.147, 0.204, 0.206 A/W and 45.57, 47.73, 30.05 %, respectively. However, for the *p*-ZnO/SiO$_2$ ultrathin interlayer/ *n*-Si photodiode, the *R* and *QE* were 0.225, 0.252, 0.297 A/W and 69.75, 58.96, 43.33 %, respec-

tively. As shown in Figure 8 (b), the use of an intermediate oxide film resulted in a greater R in the UV/visible/IR region than was measured for the p-ZnO/SiO$_2$ ultrathin interlayer/n-Si structure photodiodes. This result suggests that the intermediate oxide ultrathin film passivates surface states and increases the tunneling photocurrent, thus improving both QE and R.
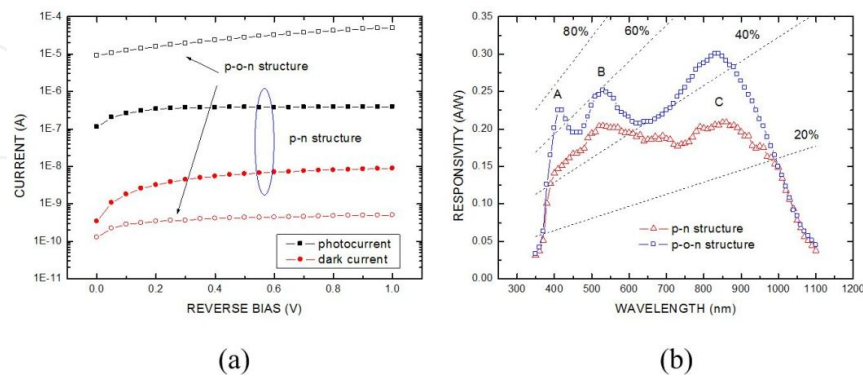

Figure 8. p-ZnO/SiO$_2$ ultrathin interlayer/n-Si and p-ZnO/n-Si structure photodiodes. (a) Dark and illuminated (λ = 530 nm) (I-V) characteristics (b) Responsivity as a function of wavelength at a bias of -1 V [49].

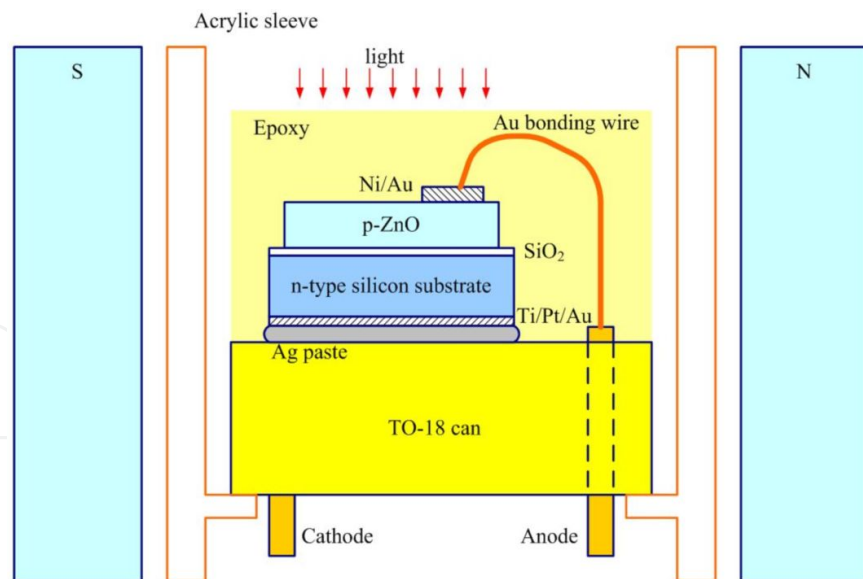## 4. ZnO/SiO$_2$/Si UV photodiodes in a strong magnetic field

Figure 9. shows the cross-section of the p-ZnO/SiO$_2$ ultrathin interlayer/n-Si structure completed configuration in a strong magnetic field [50].

In recent years, diluted magnetic semiconductors (DMSs) are attracted much great scientific interest because of their unique spintronics properties with potential technological applications. Consequently, the high Curie temperature ferromagnetism of ZnO and related materi-

als, doped with transition metal (TM) ions, is also expected to have applications in spintronics, including in information storage and data-processing devices [56]. The electronic, optical and magnetic properties of TM-doped ZnO and related materials have been studied extensively [57-64]. However, the behavior and characteristics of ZnO optoelectronic devices in a magnetic field have seldom been investigated. Photodiodes with a p-ZnO/SiO$_2$ ultrathin interlayer/n-Si structure in a magnetic field (Faraday configuration) as shown in Figure 9 were studied [50,51].

Figure 10 (a) plots the I-V characteristics of photodiodes that were measured in the dark (dark current), under illumination with a xenon arc lamp at 100 W, and in magnetic fields of 0, 0.1, 0.5 and 0.7 T, at applied reverse biases ranging from 0 to 1 V at room temperature. The magnetic field-induced photocurrents were 3.02×10^{-5}, 4.89×10^{-5}, 1.02×10^{-4}, and 2.27×10^{-4} A in magnetic fields of 0, 0.1, 0.5 and 0.7 T, respectively, at a reverse bias of 1 V. However, the dark current in various magnetic fields remains almost constant (~1.27×10^{-8} A). Evidently, the photocurrent/dark-current contrast ratios are about four orders of magnitude in magnetic field. A change of the applied magnetic field does not noticeably change the total current in the dark. However, when the photodiode was illuminated, the total current significantly increases by approximately one order of magnitude under a strong magnetic field, such as 0.7 T.

The total current can be described as

$$I_{Total} = I_{Dark} + I_{Light} + I_{Magnetism} \qquad (4)$$

where I_{Dark} is the dark current, I_{Light} is the photocurrent or photo-generated current, and $I_{Magnetism}$ is the magnetic field-induced current or magneto-induced current.
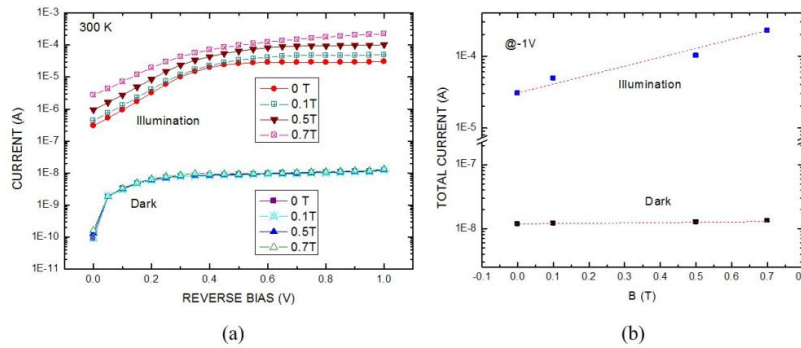

Figure 10. a) The I-V characteristics of the p-ZnO/SiO$_2$ ultrathin interlayer/n-Si structure photodiode in the dark, illuminated and under an applied magnetic field. (b) Total current at a reverse bias of 1 V against various magnetic fields [50].

Figure 10(b) a plots the total current at a reverse bias of 1 V as a function of the magnetic field. In the case of non-illumination, applying a magnetic field only slightly changed the total current because of the absence of photo-ionization. However, under illumination, $I_{Magnetism}$

exponentially increases with the applied magnetic field because the probability of photo-excitation increased [65,66]. This phenomenon is called the magneto-optical multiplication e ﬀ ect. The magneto-optical current multiplication effect may be caused by photo-ionization due to the quantized magnetic effect of ZnO film in the photodiode structure.

Figure 11(a) and 11(b) show the *I-V* characteristics of photodiodes measured under illumination with a xenon arc lamp at various operating power levels, and in a magnetic field of 0.5 T at applied reverse biases from 0 to 1 V at room temperature. Figure 11(b) depicts the magneto-induced current calculated in Eq. (4), showing that the magneto-induced current increases exponentially as the reverse bias increases. Figure 11(c) plots the photocurrent as a function of wavelength in the ranges 300-720 nm for a *p*-ZnO/SiO$_2$ ultrathin interlayer/*n*-Si structure photodiode, measured throughout this work at a reverse bias of 1 V. The current variation of the photodiode was obvious when the wavelength of incident light was lower, around 375 nm (higher photon energy). Therefore, the photo-ionization due to quantized magnetic effect of nanostructure ZnO film is apparently the source the magneto-induced current [65,66].
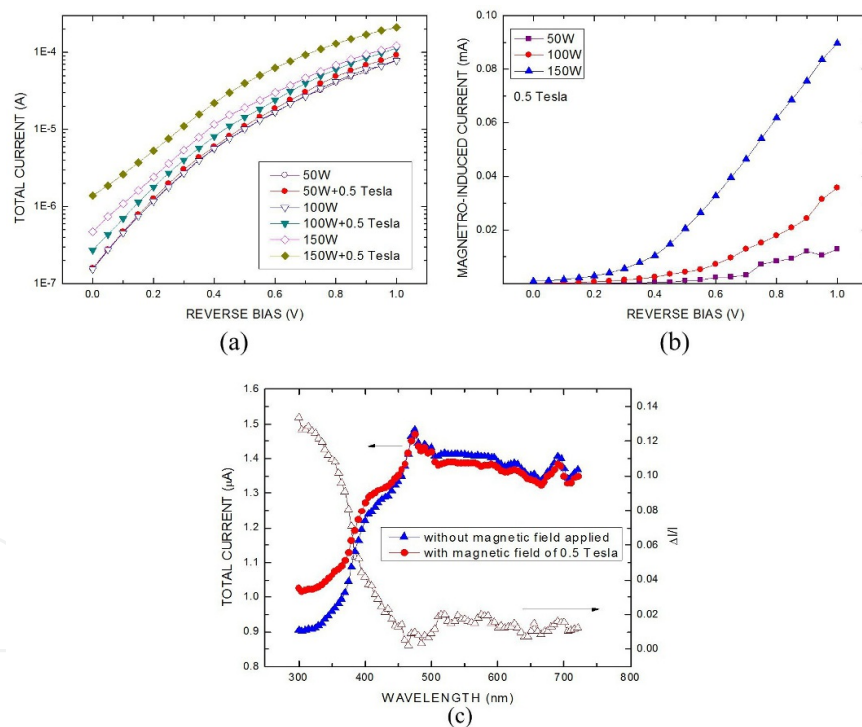

Figure 11. a) and (b) Illuminated and magnetic field applied *I-V* characteristics of the *p*-ZnO/SiO$_2$ ultrathin interlayer/*n*-Si structure photodiode with a xenon arc lamp at various operating power and magnetic field of 0.5 T applied. (c) Photocurrent as a function of wavelength in the ranges 300-720 nm [51].

Figure 12(a) plots the responsivity as a function of wavelength for a photodiode with the *p*-ZnO/SiO$_2$ ultrathin interlayer/*n*-Si structure, measured throughout this work at a reverse bias of 1 V at which the system is in a stable optoelectronic regime. Peak A located at around 410 nm is interpreted as the excitonic absorption in the ZnO film. Peak B (around 470 nm)

may be attributed to the band-to-deep level absorption in the ZnO film. Peak B (around 470 nm) may be attributed to the band-to-deep level absorption in the ZnO film. The band absorption edge of responsivity in the absence of a magnetic field is located at a wavelength of around 371 nm, which corresponds to the band-to-band absorption of the ZnO film [54]. In this work, the responsivity (R) and quantum efficiency (QE) at 410 nm under an applied magnetic field of 0.5 T are 0.25 A/W and ~76 %, respectively. R and QE at 410 nm in the absence of an applied magnetic field are 0.20 A/W and ~61 %, respectively. Therefore, Eq. (1) had to modify, R is given by [27]

$$R = I_{ph} / P_{inc} = \eta \zeta \frac{q}{h\nu} (A/W)$$
(5)

where the gain factor, ζ, is governed by the magneto-optic multiplication effect. In an applied magnetic field of 0.5 T, the band absorption edge of responsivity shifts to 370 nm. The photon energy has shifted by approximately 9.03 meV. This result suggests that the magnetic field splits the conduction-band edge into Landau levels with a spacing of $\frac{1}{2}\hbar\omega_{ce}$, and the valence-band edge into Landau levels with a spacing of $\frac{1}{2}\hbar\omega_{ch}$, as displayed in Figure 12 (b), where $\hbar$ is the reduced Planck's constant, ω_{ce} is the cyclotron resonance frequency of electrons, and ω_{ch} is the cyclotron resonance frequency of holes. Accordingly, this process is referred as the interband magneto-optic absorption due to the Landau splitting.
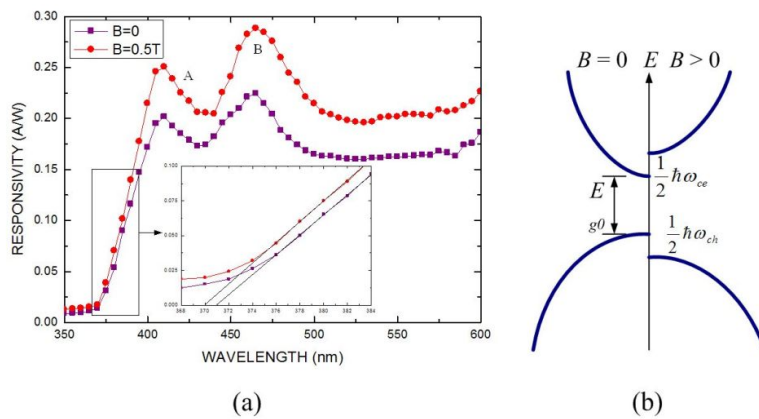

Figure 12. a) Responsivity as a function of wavelength for the photodiode with p-ZnO/SiO$_2$ ultrathin interlayer/n-Si structure at a reverse bias of 1 V. (b) Schematic band diagram to elucidate the responsivity [50].

Figure 13(a) plots the photocurrent as a function of wavelength in the range of 350-410 nm for a p-ZnO/SiO$_2$ ultrathin interlayer/n-Si structure photodiode, measured throughout this work at a reverse bias of 1 V. All spectra were normalized to clarify the photon energy shift. The absorption edge of photodiode without an applied magnetic field was at a wavelength of approximately 370.5 nm. The absorption edge of photodiode with applied magnetic field

of 0.1, 0.5, and 0.7 Tesla shifted to 370, 369, and 368.5 nm, respectively, while the photon energy shifts were approximately 4.51, 9.03, and 18.11 meV, respectively. This result suggests that the magnetic field splits the conduction-band edge into Landau levels.

Hence, according to the discussion above, a carrier transport model can be used to descript the magneto-induced current. Figure 13(b) shows that the dark current and photocurrent can be respectively described as [30,49,53]

$$I_{Dark} = I_S + I_{Tp} + I_{Tn} \tag{6}$$

and

$$I_{Light} = I_{Tn} + I_{Dn} + I_{Ln} + I_{Tp} + I_{Dp} + I_{Lp} \tag{7}$$

where J_S is the surface recombination current through the surface states, J_{Tp} is the hole tunneling current, J_{Tn} is the electron current through surface states, J_T is the tunneling current, J_D is the current in the depletion region, and J_L is the photo-generated current. The subscripts n and p indicate electron and hole, respectively. The magneto-induced current is given by

$$I_{Magnetism} = I_{Tm} + I_{Dm} + I_{Lm} \tag{8}$$

where the subscript m indicates magnetism. Therefore, in the case of non-illumination or low flux irradiations, applying a magnetic field barely changed the total current. This is because the surface recombination velocity is so fast such that the carriers cannot produce photo-ionization. However, in the case of high flux irradiations, the probability of the photo-ionization increases as the photo-generated excess carrier increases. This phenomenon is called as magneto-optical multiplication effect, and is caused by the photo-ionization due to quantized magnetic effect of nanostructure ZnO film.
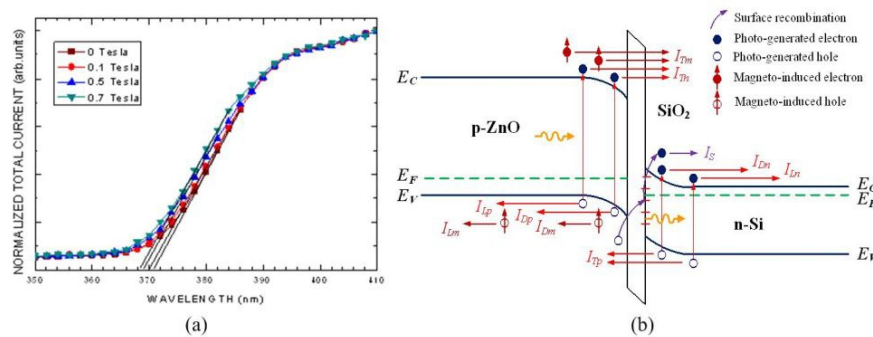

Figure 13. a) Photocurrent as a function of wavelength in the ranges 350-410 nm for a *p*-ZnO/SiO$_2$ ultrathin interlayer/*n*-Si structure photodiode (b) Schematic energy-band diagram of the *p*-ZnO/SiO$_2$ ultrathin interlayer/*n*-Si system in the presence of a magnetic field under illumination [51].

5. Conclusions

In summary, both p-ZnO/n-Si and p-ZnO/SiO$_2$ ultrathin interlayer/n-Si structures UV photodiodes have been introduced. In the aspect of p-ZnO/n-Si photodiodes, the photoresponses exhibited higher responsive regions at UV, visible and near infrared ranges. In the aspect of p-ZnO/SiO$_2$ ultrathin interlayer/n-Si photodiodes, placing in a strong magnetic field, the magneto-induced current in photodiode increases exponentially as the reverse bias and illumination flux increases, mainly because the magnetic field induced a photocurrent by magneto-optical multiplication effects. In the various magnetic fields, the absorption tails of the responsivity were shifted from 370.5 nm to 368.5 nm, and a blue shift of the photon energy from 4.52 meV to 18.16 meV were observed. This shift is attributed to the interband magneto-optical absorption caused by Landau splitting. Therefore, the magneto-optical current multiplication effect may be caused by the photo-ionization owing to quantized magnetic effect of the ZnO film. We hope all these contents may be helpful for the readers and comprehend the development of ZnO/SiO$_2$/Si UV photodiodes.

Author details

Lung-Chien Chen[*]

Department of Electro-optical Engineering, National Taipei University of Technology, 1, sec. 3, Chung-Hsiao E. Rd., Taipei 106, Taiwan, Republic of China

References

[1] Monroy, E., Calle, F., Pau, J. L., Muñoza, E., Omnès, F., Beaumont, B., & Gibart, P. (2001). AlGaN-based UV photodetectors. J. Cryst. Growth 2001; 230(3-4): 537-3.

[2] Monroy, F., Omnès, F., & Calle, F. (2003). Wide-bandgap semiconductor ultraviolet photodetectors. Semicond. Sci. Tech. 2003; 18(4): R , 33-51.

[3] Biyikli, N., Aytur, O., Kimukin, I., Tut, T., & Ozbay, E. (2002). Solar-blind AlGaN-based Schottky photodiodes with low noise and high detectivity. Appl. Phys. Lett. 2002 , 81(17), 3272-4.

[4] Lee, M. L., Sheu, J. K., Lai, W. C., Chang, S. J., Su, Y. K., Chen, M. G., Kao, C. J., Chi, G. C., & Tsai, J. M. (2003). GaN Schottky barrier photodetectors with a low-temperature GaN cap layer. Appl. Phys. Lett. 2003 , 82(17), 2913-5.

[5] Bouhdada, A., Hanzaz, M., Vigué, F., & Faurie, J. P. (2003). Electrical and optical proprieties of photodiodes based on ZnSe material. Appl. Phys. Lett. 2003 , 83(1), 171-3.

[6] Chiou, Y. Z., & Tang, J. J. (2004). GaN photodetectors with transparent indium tin oxide electrodes. Jpn. J. Appl. Phys. 2004; 43(7A): , 4146-9.

[7] Barnes, T. M., Leaf, J., Hand, S., Fry, C., & Wolden, C. A. (2004). A comparison of plasma-activated N_2/O_2 and N_2O/O_2 mixtures for use in ZnO:N synthesis by chemical vapor deposition. J. Appl. Phys. 2004 , 96(12), 7036-44.

[8] Kato, H., Sano, M., Miyanoto, K., & Yao, T. (2003). Homoepitaxial growth of high-quality Zn-polar ZnO films by plasma-assisted molecular beam epitaxy. Jpn. J. Appl. Phys. 2003; 42(2A): L , 1002-5.

[9] Pearton, S. J., Norton, D. P., Ip, K., Heo, Y. W., & Steiner, T. (2004). Recent advances in processing of ZnO. J. Vac. Sci. Technol. B 2004 , 22(3), 932-48.

[10] Zhang, X. H., Chua, S. J., Yong, A. M., Yang, H. Y., Lau, S. P., Yu, S. F., Sun, X. W., Miao, L., Tanemura, M., & Tanemura, S. (2007). Exciton radiative lifetime in ZnO nanorods fabricated by vapor phase transport method. Appl. Phys. Lett. 2007; 90(1): 013107.

[11] Danhara, Y., Hirai, T., Harada, Y., & Ohno, N. (2006). Exciton luminescence of ZnO fine particles. Phys. Stat. Sol. (c) 2006 , 3(10), 3565-8.

[12] Lim, J. H., Kang, C. K., Kim, K. K., Park, I. K., Hwang, D. K., & Park, S. J. (2006). UV electroluminescence emission from ZnO light-emitting diodes grown by high-temperature radiofrequency sputtering. Adv. Mater. 2006 , 18(20), 2720-4.

[13] Wei, Z. P., Lu, Y. M., Shen, D. Z., Zhang, Z. Z., Yao, B., Li, H., Zhang, J. Y., Zhao, D. X., Fan, X. W., & Tang, Z. K. (2007). Room temperature p-n ZnO blue-violet light-emitting diodes. Appl. Phys. Lett. 2007; 90(4): 042113.

[14] Leong, E. S. P., Yu, S. F., & Lau, S. P. (2006). Directional edge-emitting UV random laser diodes. Appl. Phys. Lett. 2006; 89(22): 221109.

[15] Lee, C. W., Choi, H., Oh, M. K., Ahn, D. J., Kim, J., Kim, J. M., Ren, F., & Pearton, S. J. (2007). ZnO-based cyclodextrin sensor using immobilized polydiacetylene vesicles. Electrochem. Solid-State Lett. 2007; 10(1): J , 1-3.

[16] Abe, T., Kashiwaba, Y., Onodera, S., Masuoka, F., Nakagawa, A., Endo, H., Niikura, I., & Kashiwaba, Y. (2007). Homoepitaxial growth of non-polar ZnO films on off-angle ZnO substrates by MOCVD. J. Cryst. Growth 2007 , 298, 457-60.

[17] Wang, X., Lu, Y. M., Shen, D. Z., Zhang, Z. Z., Li, B. H., Yao, B., Zhang, J. Y., Zhao, D. X., & Fan, X. W. (2007). Growth and photoluminescence for undoped and N-doped ZnO grown on 6H-SiC substrate. J. Lumin. 2007; 122-123: 165-7.

[18] Park, S. M., Ikegami, T., & Ebihara, K. (2006). Effects of substrate temperature on the properties of Ga-doped ZnO by pulsed laser deposition. Thin Solid Films 2006; 513(1-2) 90-4.

[19] Castañeda, L., Maldonado, A., Cheang-Wong, J. C., Terrones, M., Olvera, M., & de la , L. (2007). Composition and morphological characteristics of chemically sprayed fluorine-doped zinc oxide thin films deposited on Si(1 0 0). Physica B 2007; 390(1-2): 10-6.

[20] Kaid, M. A., & Ashour, A. (2007). Preparation of ZnO-doped Al films by spray pyrolysis technique. Appl. Surf. Sci. 2007 , 253(6), 3029-33.

[21] Bian, J. M., Li, X. M., Gao, X. D., Yu, W. D., & Chen, L. D. (2004). Deposition and electrical properties of N-In codoped p-type ZnO films by ultrasonic spray pyrolysis. Appl. Phys. Lett. 2004 , 84(4), 541-3.

[22] Chen, L. L., Ye, Z. Z., Lu, J. G., & Chu, P. K. (2006). Control and improvement of p-type conductivity in indium and nitrogen codoped ZnO thin films. Appl. Phys. Lett. 2006; 89(25): 252113.

[23] Ye, H. B., Kong, J. F., Shen, W. Z., Zhao, J. L., & Li, X. M. (2007). Origins of shallow level and hole mobility in codoped p-type ZnO thin films. Appl. Phys. Lett. 2007; 90(10): 102115.

[24] Dutta, M., & Basak, D. (2008). p-ZnO/n-Si heterojunction: Sol-gel fabrication, photo-response properties, and transport mechanism. Appl. Phys. Lett. 2008; 92(21): 212112.

[25] Chen, L. C., & Pan, C. N. (2008). P-ZnO/n-Si photodiodes prepared by ultrasonic spraying pyrolysis method. The Open Crystallography Journal 2008 , 1, 10-3.

[26] Bae, H. S., & Im, S. (2004). Ultraviolet detecting properties of ZnO-based thin film transistors. Thin Solid Films 2004; 469-470: 75-9.

[27] Sze S.M. (1981). Physics of Semiconductor Devices New York: Wiley; 1981.

[28] Um, H. D., Moiz, S. A., Park, K. T., Jung, J. Y., Jee, S. W., Ahn, C. H., Kim, D. C., Cho, H. K., Kim, D. W., & Lee, J. H. (2011). Highly selective spectral response with enhanced responsivity of n-ZnO/p-Si radial heterojunction nanowire photodiodes. Appl. Phys. Lett. 2011; 98(3): 033102.

[29] Soci, C., Zhang, A., Xiang, B., Dayeh, S. A., Aplin, D. P. R., Park, J., Bao, X. Y., Lo, Y. H., & Wang, D. (2007). ZnO nanowire UV photodetectors with high internal gain. Nano Lett. 2007 , 7(4), 1003-9.

[30] Hsu, B. C., Liu, C. W., Liu, W. T., & Lin, C. H. (2001). A PMOS tunneling photodetector. IEEE Trans. Electron Devices 2001 , 48(8), 1747-9.

[31] Mohamad, W. F., Hajar, A. A., & Saleh, A. N. (2006). Effects of oxide layers and metals on photoelectric and optical properties of Schottky barrier photodetector. Renew. Energy 2006 , 31(10), 1493-503.

[32] Wang, T. M., Chang, C. H., & Hwu, J. G. (2006). Enhancement of temperature sensitivity for metal-oxide-semiconductor (MOS) tunneling temperature sensors by utilizing hafnium oxide (HfO_2) film added on silicon dioxide (SiO_2). IEEE Sens. J. 2006 , 6(6), 1468-72.

[33] Ruddell, F. H., Montgomery, J. H., Gamble, H. S., & Denvir, D. (2007). Germanium MOS technology for infra-red detectors. Nucl. Instrum. Meth. A 2007; 573(1-2): 65-7.

[34] Kaliwoh, N., Zhang, J. Y., & Boyd, I. W. (2000). Ultrathin silicon dioxide films grown by photo-oxidation of silicon using 172 nm excimer lamps. Appl. Surf. Sci. 2000 , 168(14), 288-91.

[35] Morita, S., Shinozaki, A., Morita, Y., Nishimura, K., Okazaki, T., Urabe, S., & Morita, M. (2004). Tunneling current through ultrathin silicon dioxide films under light exposure. Jpn. J. Appl. Phys. 2004; 43(11B): , 7857-60.

[36] Mur, P., Semeria, M. N., Olivier, M., Papon, A. M., Leroux, C., Reimbold, G., Gentile, P., Magnea, N., Baron, T., Clerc, R., & Ghibaudo, G. (2001). Ultra-thin oxides grown on silicon (1 0 0) by rapid thermal oxidation for CMOS and advanced devices. Appl. Surf. Sci. 2001; 175-176: 726-33.

[37] Ueno, T., Morioka, A., Chikamura, S., & Iwasaki, Y. (2000). Low-temperature and low-activation-energy process for the gate oxidation of Si substrates. Jpn. J. Appl. Phys. 2000; 39(4B): L , 327-9.

[38] Choi, Y. W., & Ahn, B. T. (1999). A study on the oxidation kinetics of silicon in inductively coupled oxygen plasma. J. Appl. Phys. 1999 , 86(7), 4004-7.

[39] Ray, S. K., Maiti, C. K., & Chakraborti, N. B. (1990). Low-temperature oxidation of silicon in microwave oxygen plasma. J. Mater. Sci. 1990 , 25(5), 2344-8.

[40] Niimi, H., & Lucovsky, G. (1998). Ultrathin oxide gate dielectrics prepared by low temperature remote plasma-assisted oxidation. Surf. Coat. Technol. 1998; 98(1-3): 1529-33.

[41] Zhang, J. Y., & Boyd, I. W. (1997). Low temperature photo-oxidation of silicon using a xenon excimer lamp. Appl. Phys. Lett. 1997 , 71(20), 2964-6.

[42] Chang, H. S., Choi, S., Moon, D. W., & Hwang, H. (2002). Improved reliability characteristics of ultrathin SiO_2 grown by low temperature ozone oxidation. Jpn. J. Appl. Phys. 2002 , 41(10), 5971-3.

[43] Tosaka, A., Nishiguchi, T., Nonaka, H., & Ichimura, S. (2005). Low-temperature oxidation of silicon using UV-light-excited ozone. Jpn. J. Appl. Phys. 2005; 44(37-41): L , 1144-6.

[44] Hwang, C. C., An, K. S., Park, R. J., Kim, J. S., Lee, J. B., Park, C. Y., Kimura, A., & Kakizaki, A. (1999). Alkali metal promoted oxidation of the Si(113) surface. Thin Solid Films 1999 , 341(1), 156-9.

[45] Uchikoga, S., Lai, D. F., Robertson, J., Milne, W. I., Hatzopoulos, N., Yankov, R. A., & Weiler, M. (1999). Low-temperature anodic oxidation of silicon using a wave resonance plasma source. Appl. Phys. Lett. 1999 , 75(5), 725-7.

[46] Bertagna, V., Erre, R., Saboungi, M. L., Petitdidier, S., Lévy, D., & Menelle, A. (2004). Neutron reflectivity study of ultrathin SiO_2 on Si. Appl. Phys. Lett. 2004 , 84(19), 3816-8.

[47] Kailath, B. J., Das, Gupta. A., & Das, Gupta. N. (2007). Electrical and reliability characteristics of MOS devices with ultrathin SiO_2 grown in nitric acid solutions. IEEE Trans. Device Mater. Reliab. 2007 , 7(4), 602-10.

[48] Kim, W. B., Matsumoto, T., & Kobayashi, H. (2010). Ultrathin SiO_2 layer with a low leakage current density formed with ~ 100% nitric acid vapor. Nanotechnology 2010; 21(11): 115202.

[49] Chen, L. C., & Pan, C. N. (2008). Photoresponsivity enhancement of ZnO/Si photodiodes through use of an ultrathin oxide interlayer. Eur. Phys. J. Appl. Phys. 2008 , 44(1), 43-6.

[50] Chen, L. C., & Lu, M. I. (2009). Magneto-optical multiplication effects in $ZnO/SiO_2/Si$ photodiodes. Scr. Mater. 2009 , 61(8), 781-4.

[51] Chen, L. C., & Tien, C. H. (2010). Photocurrent properties of nanostructered ZnO/SiO_2/Si photodiodes in magnetic fields. Curr. Nanosci. 2010 , 6(4), 397-401.

[52] Jeong, I. S., Kim, J. H., & Lm, S. (2003). Ultraviolet-enhanced photodiode employing n-ZnO/p-Si structure. Appl. Phys. Lett. 2003 , 83(14), 2946-8.

[53] Doghish, M. Y., & Ho, F. D. (1993). A comprehensive analytical model for metal-insulator-semiconductor (MIS) devices: a solar cell application. IEEE Trans. Electron Devices 1993 , 40(8), 1446-54.

[54] Wang, X. H., Yao, B., Shen, D. Z., Zhang, Z. Z., Li, B. H., Wei, Z. P., Lu, Y. M., Zhao, D. X., Zhang, J. Y., Fan, X. W., Guan, L. X., & Cong, C. X. (2007). Optical properties of p-type ZnO doped by lithium and nitrogen. Solid State Commun. 2007 , 141(11), 600-4.

[55] Xiu, F. X., Yang, Z., Mandalapu, L. J., Zhao, D. T., & Liu, J. L. (2005). Photoluminescence study of Sb-doped p-type ZnO films by molecular-beam epitaxy. Appl. Phys. Lett. 2005; 87(25): 252102.

[56] Dietl, T., Ohno, H., Matsukura, F., Cibert, J., & Ferrand, D. (2000). Zener Model description of ferromagnetism in Zinc-blende magnetic semiconductors. Science 2000 , 287(5455), 1019-22.

[57] Ohno, H., Chiba, D., Matsukura, F., Omiya, T., Abe, E., Dietl, T., Ohno, Y., & Ohtani, K. (2000). Electric-field control of ferromagnetism. Nature 2000 , 408, 944-6.

[58] Samanta, K., Bhattacharya, P., Duque, J. G. S., Iwamoto, W., Rettori, C., Pagliuso, P. G., & Katiyar, R. S. (2008). Optical and magnetic properties of $Zn_{0.\ -x}Co_{0.1}O : Al_x$ thin films. Solid State Commun. 2008; 147(3-4): 305-8., 9 .

[59] Zou, W. Q., Mo, Z. R., Lu, Z. L., Lu, Z. H., Zhang, F. M., & Du, Y. W. (2008). Magnetic and optical properties of $Zn_{-x}Co_xO$ thin films prepared by plasma enhanced chemical vapor deposition. Physica B 2008; 403(19-20): 3686-8., 1.

[60] Chen, W. M., Buyanova, I. A., Murayama, A., Furuta, T., Oka, Y., Norton, D. P., Pear-
ton, S. J., Osinsky, A., & Dong, J. W. (2008). Dominant factors limiting efficiency of
optical spin detection in ZnO-based materials. Appl. Phys. Lett. 2008; 92(9): 092103.

[61] Behan, A. J., Neal, J. R., Ibrahim, R. M., Mokhtari, A., Ziese, M., Blythe, H. J., Fox, A.
M., & Gehring, G. A. (2007). Magneto-optical and transport studies of ZnO-based di-
lute magnetic semiconductors. J. Magn. Magn. Mater. 2007 , 310(2), 2158-60.

[62] Ivanov, V. Y., Godlewski, M., Yatsunenko, S., Khachapuridze, A., Golacki, Z., Sa-
wicki, M., Omel'chuk, A., Bulany, M., & Gorban, A. (2004). Optical and magnetic res-
onance investigations of ZnO crystals doped with TM ions. Phys. Stat. Sol. (c) 2004 ,
1(2), 250-3.

[63] Lambrecht, W. R. L., Rodina, A. V., Limpijumnong, S., Segall, B., & Meyer, B. K.
(2002). Valence-band ordering and magneto-optic exciton fine structure in ZnO.
Phys. Rev. B 2002; 65(7): 075207.

[64] Thota, S., Kukreja, L. M., & Kumar, J. (2008). Ferromagnetic ordering in pulsed laser
deposited $Zn_{1-x}Ni_xO/ZnO$ bilayer thin films. Thin Solid Films 2008 , 517(2), 750-4.

[65] Tzeng, S. Y. T., & Tzeng, Y. (2004). Two-level model and magnetic field effects on the
hysteresis in n-GaAs. Phys. Rev. B 2004; 70(8): 085208.

[66] Wang, F. P., Monemar, B., & Ahlstrom, M. (1989). Mechanisms for the optically de-
tected magnetic resonance background signal in epitaxial GaAs. Phys. Rev. B 1989 ,
39(15), 11195-8.